Proceedings World Geothermal Congress 2020+1
Reykjavik, Iceland, April - October 2021

# Correlation Function $\Gamma_{meq}(r) \sim 1/r^{1/2}$ Coupling of Microseismicity to Permeability -- the Basis for Fluid Flow Seismic Image Targeting for Geothermal Production Wells

Peter Leary & Peter Malin

Advanced Seismic Instrument & Research, 1311 Waterside, Dallas, TX 75218-4475, USA
Email: pcl@asirseismic.com

**Keywords:** MEQ, microseismicity, spatial correlation, permeability, stimulation, fractures, fluid flow

**ABSTRACT**

Direct association of microseismicity with crustal fluid flow properties has long been assumed, but for a variety of reasons it has been difficult to define a close spatial association using subsurface measurements. We show here that a pervasive rock-fluid interaction is naturally expressed in terms of a critically stressed brittle crust exhibiting power-law scaling distributions of poroperm properties. This rock-fluid interaction gives rise to a power-law scaling spatial correlation relation for induced and ambient microearthquake event locations. In mathematical terms, observed multi-scale microseismic event clustering described by two-point spatial correlation function $\Gamma_{meq}(r) \sim 1/r^{1/2}$ can be derived from two widely attested empirical poroperm relations. These empirical relations are (i) power-law spectral scaling of crustal porosity well-log sequences $\varphi(:)$, $S_\varphi(k) \sim 1/k$ over five decades of scale length $1/\text{km} < k < 1/\text{cm}$; and (ii) well-core evidence for permeability distributions given by $\kappa \sim \exp(\alpha\varphi)$, where empirical parameter $\alpha$ has values such that the mean exponent value is tightly bounded, $3 < \alpha\underline{\varphi} < 4$, across the two decades of mean porosity range $0.003 < \underline{\varphi} < 0.3$ ranging from deep basement crystalline rock to standard crustal reservoir rock including hydrogeothermal systems.

The established spatial correlation function for induced and ambient seismicity $\Gamma_{meq}(r) \sim 1/r^{1/2}$ is numerically predicted by applying the Wiener-Khinchin theorem to wide-sense stationary randomly fluctuating poroperm media, $P(k) \sim \int \exp(ikr)\Gamma(r)dr$. This general expression directly relates power-law scaling crustal poroperm fluctuation spectral power $P(k)$ to the empirical power-law scaling microseismicity spatial correlation function $\Gamma_{meq}(r) \sim 1/r^{1/2}$. More particularly, arbitrary numerical simulation of 3D permeability volumes can be generated for the complete range porosity spatial correlation conditions $P_\varphi(k) \sim 1/k^m$ from $m \sim 0$ for low spatial correlation (white or Gaussian) spatial noise to $m \sim 2$ for high spatial correlation (red or Brownian) spatial noise. The two-point spatial correlation functions $\Gamma_\kappa(r) \sim 1/r^n$ computed across the $0 < m < 2$ sequence of simulation permeability volumes indicate that exponent $n \sim ½$ occurs for porosity spatial correlation scaling exponent $m \sim 1$, the value seen universally in crustal well-logs for deep basement rock to standard crustal reservoir rock, $0.003 < \underline{\varphi} < 0.3$.

From the Wiener-Khinchin relation, we may deduce that the observed correlation property $\Gamma_{meq}(r) \sim 1/r^{1/2}$ for induced and ambient seismicity is a statistical indication that microseismic slip events occur in close spatial association with the ability of fluid to flow within a crustal volume. A close spatial association of naturally occurring fluid flow pathways with low-level energy seismic release has been extensively observed in shale formations undergoing frack-stimulation. It is logical to infer that where $\Gamma_{meq}(r) \sim 1/r^{1/2}$ microseismicity correlation is observed, there is an underlying crustal permeability distribution corresponding to fracture-connectivity fluid flow systems that continuously emit lower-level seismic energy that can be remotely detected and mapped by surface seismic sensor arrays. Such fluid flow maps of convective geothermal flow systems can be used to guide production well drilling to intersect large-scale convective flow structures.

## 1. INTRODUCTION

The controlling features of a convective geothermal resource may be expressed as $Q/\rho C = VT$, showing that the wellbore-extracted heat flow $Q$ is proportional to both the volumetric flow rate $V$ and the temperature $T$ of water passing through production wellbores. While T and V play equal roles in physically defining the commercial worth of wellbores, geothermal resource exploration has historically paid great attention to assessing $T$ and little attention to assessing $V$. This matters: while smooth diffusion temperature fields T offer broad drilling targets, wellbore production flow V is highly uncertain due to the spatially erratic and unpredictable nature of crustal flow structures. At present, a great deal of costly exploration drilling is required to establish the flow structure of convective geothermal flow systems [1]. We think that this situation is about to change, allowing as much exploration attention to $V$ as to $T$.

Our reasoning is based on two developments. First, it is now understood how crustal flow systems are defined by strong spatially erratic clustering in marked contrast to smooth disseminated temperature fields [2-9]. Second, seismic array acquisition and processing technology now exists to remotely detect flow system structural clustering [10-14]. Recognising both the clustering nature of crustal fluid flow and the ability to remotely map flow clustering gives convective geothermal resource operators the chance to manage drilling uncertainty caused by erratic $V$-structures. Accurate flow structure maps of convective geothermal flow systems allow operators to drill high productivity wells much sooner in their field development. The cost saving of ''smart'' drilling reduces capital costs for operating and sustaining field production, and opens the door to bringing smaller geothermal systems into commercial operation.

In this this paper we seek to underpin the demonstrated seismic array detection of crustal flow clustering by linking the spatial distribution of crustal flow properties to the spatial distribution of induced and naturally occurring crustal microseismicity. We show that the spatial clustering systematics of crustal flow systems attested in well-log, well-core and well-productivity data are directly related to how induced and ambient crustal microseismicity is distributed within generic crustal volumes. Physically linking crustal microseismicity to crustal permeability explains how continuously emitted sub-microseismic seismic energy – i.e., ''nano-seismicity'', even ''pico-seismicity'' – generated by geothermal flow systems can be detected and accurately mapped to identify

where flow clustering is concentrating convective flow pathways. Abundant nano-seismic to pico-seismic data associated with fluid injection have been recorded at 6km depth in Fennoscandian basement rock [15].

The spatial clustering nature of crustal flow systems derives from the spatial correlation properties of crustal porosity and permeability directly recorded by well-logs and well-cores and seen in well-productivity statistics. In particular, we can see that the amplitude of spatially correlated crustal poroperm properties scales as a power-law of the flow system dimension [2-3]. The greater the flow system dimension, the greater the flow system capacity and hence the greater the consequence of spatial clustering for resource operators. At the same time, we see that induced and ambient crust microseismic event locations are also spatially correlated as a power-law in offset between events [9]. In a scale-independent manner, the closer two microseismic events are, the greater the probability that the two events share a common permeability structure. The observed microseismicity spatial correlation systematics mean that crustal induced and ambient microseismicity distributions are subject to physical control by crustal poroperm property distributions.

Physically connecting crustal poroperm distributions and crustal microseismicity distributions does not, however, equate to discrete and episodic microseismicity events acting as an effective map of fluid flow continuity structures. Crustal fluid flow is physically defined by conservation of fluid mass, and as such fluid flow is both time- and space-continuous rather than time- and space-episodic in the manner of microseismicity. Essential for seismic mapping of crustal flow structures are the nano-scale-to-pico-scale seismic energy emissions continuously emitted by spatially connected fluid-flow pathways. Nano-to-pico-scale seismic emissions are too small and too continuous to appear as discrete events on seismic sensors.

Present day seismic array data acquisition and processing can overcome the small amplitude of nano-to-pico-scale seismic energy emission if the seismic energy is steadily generated over extended periods of time. Small-scale continuous seismic signal generation is now routinely detected and processed for hydrocarbon-bearing shale formations [11-14]. Detection of low-level seismic energy emission reveals the presence of large-scale fracture-connectivity flow systems by which most crustal fluid mass moves through geological formations. As low-level seismicity in shale formations is associated with largely immobile crustal fluids, it is logical to expect that high mobility convective geothermal fluid flow are strong generators of background seismic energy emission. In activating seismic scaling arguments for nano- and pico-scale emission associated with fluid flow, we bring physical plausibility and conceptual clarity to the use of continuous multi-channel seismic array recording and processing as means of locating production well drilling targets in convective geothermal flow systems.

Our discussion begins with contrasting the long-standing quasi-uniformity approach to crustal fluid flow against the abundant evidence that crustal fluid flow is highly non-uniform. In the context of non-uniform flow, the physical importance of flow connectivity is illustrated by applying conservation of fluid mass to flow in randomly fluctuating spatially-correlated permeability structures. We see via numerical models how non-uniform filamentary fracture-connectivity flow structures are an elementary feature of the crust. Numerical examples of spatially-correlated flow continuity structures set the scene for introducing two-point spatial correlation functions to identify the spatial correlations occurring in crustal stochastic property distributions. The two-point correlation functions identify the power-law scaling spatial-correlation nature of induced and ambient microseismicity that is imposed by the spatial correlation properties of crustal flow. Noting that the Wiener-Khinchin theorem for stochastic systems connects generic spatial spectral properties of crustal poroperm distributions to generic spatial correlation properties of microseismicity [16], we numerically demonstrate that the specifics of poroperm spatial correlation imply the specifics of microseismicity spatial correlation. Having identified the spatial correlation nature of discrete microseismicity associated with fluid flow [15,17], we can infer the existence of continuous nano-seismic to pico-seismic signal generation by convective flow geothermal systems.

## 2. FLUID FLOW CONNECTIVITY IN SPATIALLY CORRELATED CRUSTAL POROPERM DISTRIBUTIONS

Flow of crustal fluids is a stochastic process in the sense that crustal fluids make their way through assemblages of pores within a matrix of solid mineral grains whose spatial distributions are unknown and unknowable. In the absence of specific knowledge about pore distributions, and equally or more important, knowledge about how pores are connected to form permeability, the long-standing tradition in geology and geophysics dating from the 1930s has been to assume that pore and grain distributions in crustal rock are random in the simplest, most unstructured way [18-23].

The simplest, most unstructured form of randomness is defined by the condition of each pore or grain being independent of the condition of all other grains and pores. From a statistical perspective, the details of the physical process by which fluids flow from pore to pore through a granular assemblage are less important than the condition that the local flow condition at point A does not affect, nor is affected by, the local flow condition at point $B \neq A$. If the statistical independence condition is met in crustal rock, then the central limit theorem can be appealed to for assurance that the flow properties of crustal rock are normally distributed about a stable mean value within a stable deviation from the mean. This statistical framework has become deeply embedded in crustal reservoir conceptual and computational modelling and management decision making [24].

It happens, however, that this long-standing and deeply entrenched approach to randomness in crustal flow properties is profoundly wrong. Overwhelming evidence from well-logs, well-core and well-production shows that crustal grains and crustal fluids interact at all scale lengths to generate spatially-correlated flow-connectivity fluid percolation pathways and that these pathways can spatially cluster in erratic ways at all scale lengths [1-9]. Spatial correlation effects are directly or indirectly observed in well-logs and well-core from the mm-scale (grains) to km-scale (reservoirs). While the physical details of such interactions are hugely complex, the statistical picture is dominated by the simple fact that rock-fluid interactions create a statistical bias in which the local flow properties at a point A have a distinct spatial correlation with local flow properties at point $B \neq A$.

What is more, there is plentiful evidence that statistical correlation bias effects are scale-independent rather than scale-dependent [2-3]. A crustal volume of size X affects neighbour volumes of size X to the same degree and in the same manner as a crustal value of size F*X affected neighbour volumes of size F*X, where scale factor F can range over six orders of magnitude in crustal rock-fluid interactions. E.g., if crustal scale volume X = 1 meter, then the scaling factor F can range from 1/1000 to 1000.

The root observational basis for spatial correlation phenomena in crustal flow systems are the following three empirical conditions:

I. Well-logs: Crustal porosity fluctuation power scales inversely as a power-law in spatial frequency $k$, $P_\varphi(k) \sim 1/k$ [2-3];
II. Well-core: Spatial variations in well-core permeability $\kappa$ closely track well-core porosity as $\delta\log(\kappa) \sim \alpha\delta\varphi$ [4,8];
III. Well productivity: Parameter $\alpha$ in (II) has values such that $\alpha\underline{\varphi} \sim 3\text{-}4$ across formation mean porosity range $0.001 < \underline{\varphi} < 0.3$; for this empirical condition, well-productivity distributions $\kappa \sim \exp(\alpha\varphi)$ are formally lognormal in agreement with well flow data for all crustal fluid systems [1,4-7].

The foundational spatial correlation empirics (I)-(III) of crustal flow systems violate the condition for the central limit theorem. For instance, the lognormal empirics of well-core permeability and well-productivity are incompatible with a physical system in which statistically independent processes generate only normal distributions. Less obvious but equally important, the central limit theorem dependence on uncorrelated randomness requires that the fluctuation power-spectrum of, say, crustal porosity spatial fluctuation power be independent of spatial frequency, $P_\varphi(k) \sim 1/k^0 \sim const$. This condition directly and markedly contrasts with the highly attested empiric (I) that porosity fluctuation power scales inversely with spatial frequency. In light of (I)-(III), crustal systems require statistical methods that are compatible with spatially correlated rather than spatially uncorrelated physical processes

Fortunately, the physical empirics of crustal fluid flow processes (I)-(III) are easily expressed in numerical form, and we can use numerical constructs as a basis for physical and statistical discussions. For a statistical perspective on crustal flow empirics, we do not need an exhaustive account of microscale physical flow processes. Rather, we need only capture the spatial correlation properties of crustal flow.

The essence of spatial correlation is illustrated in Fig 1, which compares fluid flow stream lines for uncorrelated spatial randomness (left) with fluid flow stream lines for spatially-correlated randomness (right). Visual inspection shows that spatially uncorrelated random flow structures on the left can be statistically treated on all scales as having a stable mean value with a stable deviation from the mean. That statistical stability conspicuously does not hold for the spatially correlated flow structures on the right. For spatially correlated flow distributions, knowledge of the statistical mean and median flow properties provide no guide to where in the crustal section flow is strongest, e.g., where a reservoir operator might wish to drill a production well.

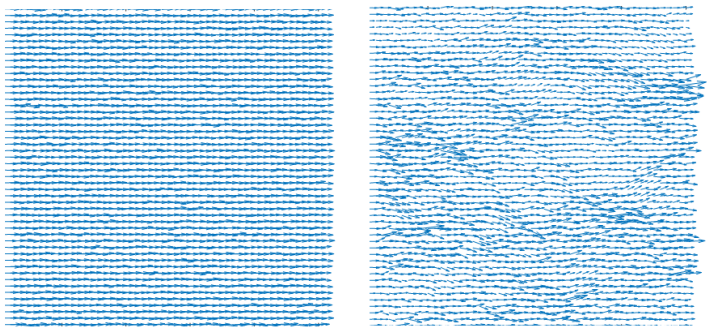

**Figure 1: Streamline fluid flow through a quasi-uniform, spatially-uncorrelated 2D permeability structure (left) and a spatially-correlated 2D permeability structure (right). A driller would have no difficulty in locating production wells in a crustal volume with uncorrelated flow distribution (left), but would be subject to large uncertainties in locating suitably productive wells in the presence of flow-heterogeneity (right). Driller uncertainty would be greatly eased with a flow heterogeneity map.**

A more quantitative understanding the impact of spatial correlation in crustal media comes via Darcy's law of fluid flow, $\boldsymbol{v} = \kappa/\mu\nabla P$. An essential property of fluid flow is material continuity expressed by the conservation of mass condition $\nabla\cdot\boldsymbol{v} = 0$, saying that the sum of fluid flow into and out of a crustal volume must sum to zero. Combining these two physical statements gives the fluid flow condition $\nabla\cdot(\kappa/\mu\,\nabla P) = 0$, with expanded form $\nabla^2 P = -1/\kappa\,\nabla\kappa\cdot\nabla P$. As is familiar from the history of core-scale fluid flow investigations and reservoir-scale flow simulation [18-23,25-27], it has been routine to ignore the RHS of this expression, reducing the fluid pressure field to a potential equation, $\nabla^2 P = 0$. The standard approximation to crustal reality conveniently puts fluid pressure on the same footing as temperature, $\nabla^2 T = 0$, as derived from Fourier's law of thermal conduction in solids. Ignoring the spatial correlation property of crustal media opened the door to a century of mathematic techniques for the potential equation by which to describe fluid flow in the crust [20,25].

We must ask, however, what happens if, as in the right-hand side of Fig 1, the gradient of spatially fluctuating permeability in the term $-1/\kappa\,\nabla\kappa\cdot\nabla P$ cannot be dismissed. The once uncomplicated pressure field equation $\nabla^2 P = 0$ now becomes $\nabla^2 P = -1/\kappa\,\nabla\kappa\cdot\nabla P$, essentially intractable to all but numerical methods which can handle the stochastic nature of spatially fluctuating crustal permeability described by empirics (I)-(III).

Coming to grips with spatial correlation properties of physical systems requires new statistical tools, in this case the application of spatial correlation functions. The simplest spatial correlation function $\Gamma(r)$ measures the population distribution as a function of incremented distance $r$ separating pairs of ''events'' within a crustal volume [28-30; Appendix]. While we immediately can see that $\Gamma(r)$ for an uncorrelated random distribution of points (Fig 1 left) is independent of the distance between points, $\Gamma(r) \sim const$, it is of great interest that $\Gamma(r)$ for distributions of ''events'' relevant to spatially correlated flow structures (Fig 2 right) is a power-law $\Gamma(r) \sim 1/r^n$, $n > 0$. The two-point $\Gamma(r)$ power-law for Fig 1 (right) says that, at every scale length, ''events'' tend to cluster, i.e., have smaller inter-event offsets than would be expected for a quasi-uniform flow medium. Such flow distribution heterogeneity requires a clear physical explanation in order to respond to the reservoir operation problem its poses.

The utility of the two-point correlation function $\Gamma(r)$ is greatly increased by the Wiener-Khinchin theorem which establishes a Fourier transform pair between correlation functions $\Gamma(r)$ in spatial variable $r$ and spatial fluctuation power spectra $P(k)$ in spatial frequency $k$ [16]. The Fourier transform duality pair for the two-point correlation function can be expressed by $P(k) \sim \int exp(ikr)\Gamma(r)dr$ and its inverse $\Gamma(r) \sim \int exp(-ikr)P(k)dk$. Applying Wiener-Khinchin duality to the observed spatial correlation function of microseismicity and the empirical spectral correlation properties derived from (I)-(III) provides a cogent physical explanation for the observed microseismicity correlation $\Gamma(r) \sim 1/r^n$, $n \sim ½$.

## 3. TWO-POINT SPATIAL CORRELATION POWER-LAW SCALING FOR INDUCED AND AMBIENT MICROSEISMICITY

As indicated in Fig 1, spatially uncorrelated random property distributions have only incidental clustering, while correlated random spatial distribution can show marked degrees of spatial clustering. Fig 2 illustrates different degrees of spatial clustering for crustal permeability distributions according to empirics (I)-(III). In the two panels, the same number of 'events' occur across the same display area, but where the spatially uncorrelated permeability ''events'' at left are only incidentally adjacent, on the right spatially correlated ''events'' are strongly clustered. Fig 3 evaluates the two-point spatial correlation function $\Gamma(r)$ on these two ''event'' distributions. A Matlab-implemented correlation function for 2D event distributions is appended. The two-point correlation function power-law scaling exponent for Fig 2 cases, $n \sim 1/6$ (left) and $n \sim 3/4$ (right) reflect the degree of clustering relative to a flat line, $n = 0$.

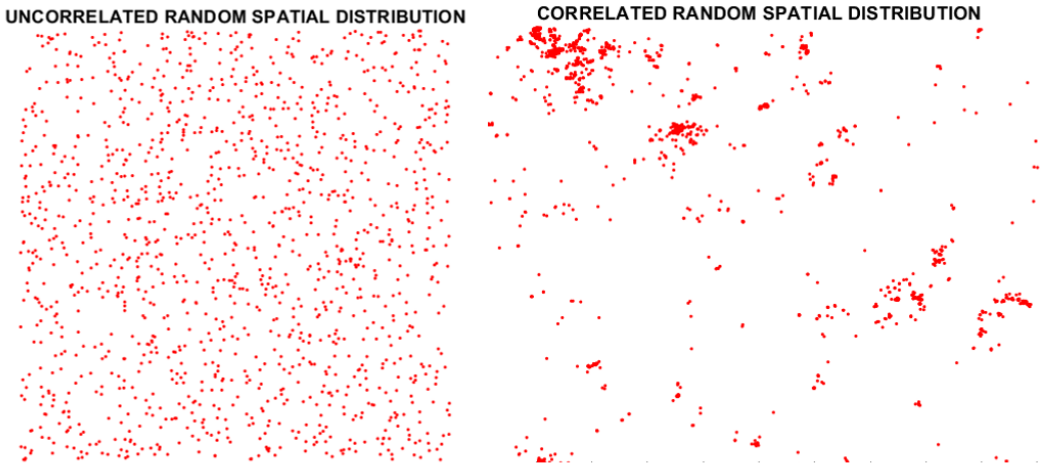


**Figure 2: Spatial distributions of uncorrelated random ''events'' (left) and correlated random ''events'' (right). Uncorrelated randomness has no systematic spatial clustering, while correlated random events are systematically clustered.**

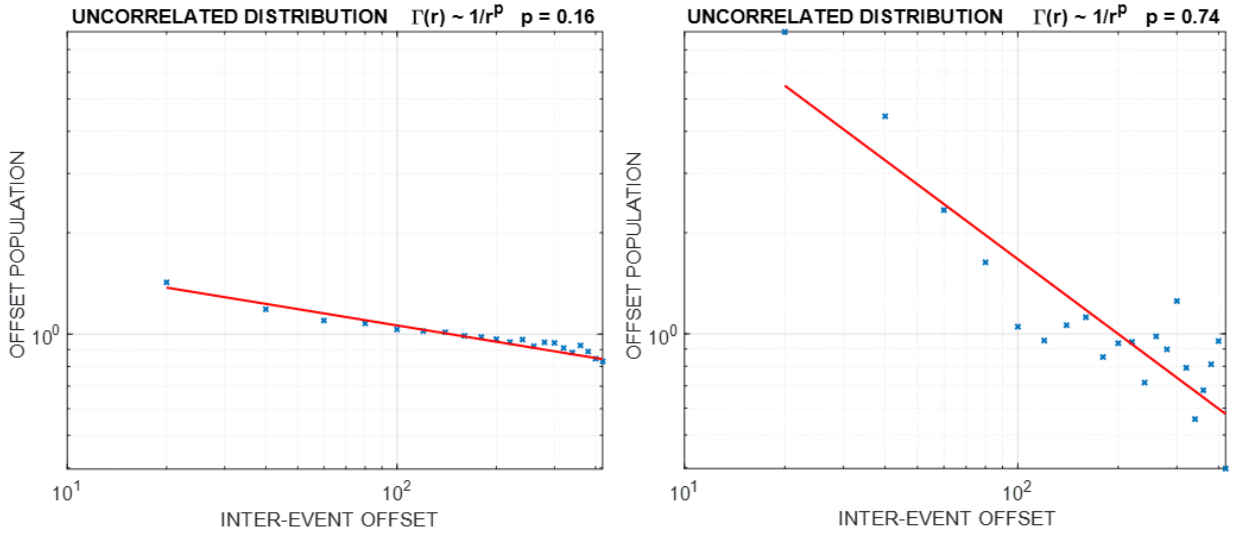


**Figure 3: Power-law scaling two-point spatial correlation functions $\Gamma(r) \sim 1/r^n$ for Fig 2 distributions of uncorrelated random ''events'' (left) and correlated random ''events'' (right). The uncorrelated spatial distribution has an essentially flat correlation function, while the cluster nature of correlated distribution forces the spatial fluctuation function to fall off steeply with inter-event distance.**

For comparison with the synthetic uncorrelated and correlated data of Fig 2, Fig 4 shows two sets of microseismic event distributions. The left-hand microseismic data are from fluid injection at 6km depth in Finnish basement rock [15]. The right-hand ambient microseismic data are from 2-3km depth in an Indonesian geothermal field [17]. Both microseism distributions have a degree of clustering greater than uncorrelated randomness but less than the Fig 2 example of correlated random noise. The two-point correlation function power-law scaling exponent for the two Fig 4 induced and ambient seismicity cases $p \sim ½$, are intermediate to the Fig 2 synthetic flow distributions.

Fig 5 shows that the Fig 4 microseismic distributions projected onto a median plane are power-law scaling, $\Gamma(r) \sim 1/r^p$, with a power-law exponent approximate one-half, $p \sim ½$. Experimentation with effects of projecting a well-behaved volume distribution onto a median plane shows that projection does not significantly bias the two-point spatial correlation function scaling exponent.

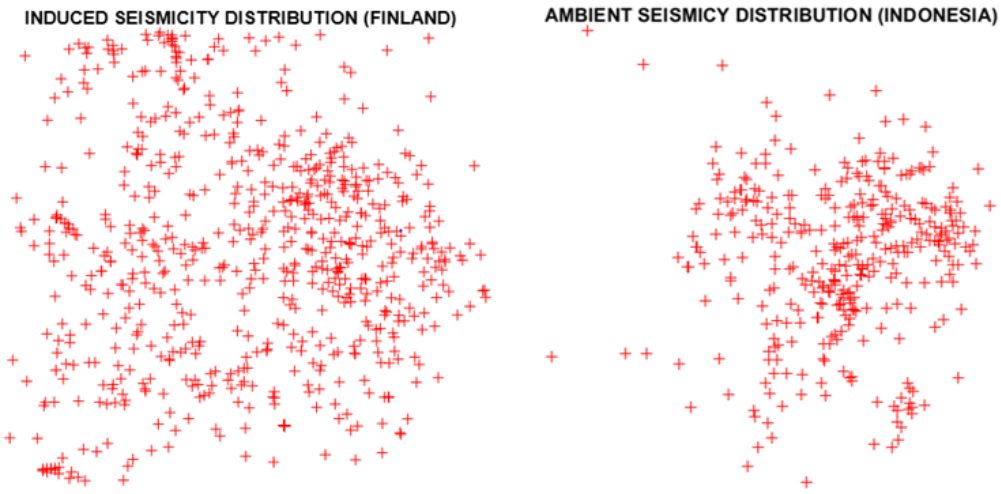


**Figure 4: Spatial distributions of induced seismic in Finnish basement (left, [15]) and ambient seismicity in a convective geothermal field in Indonesia (right, [17]).**

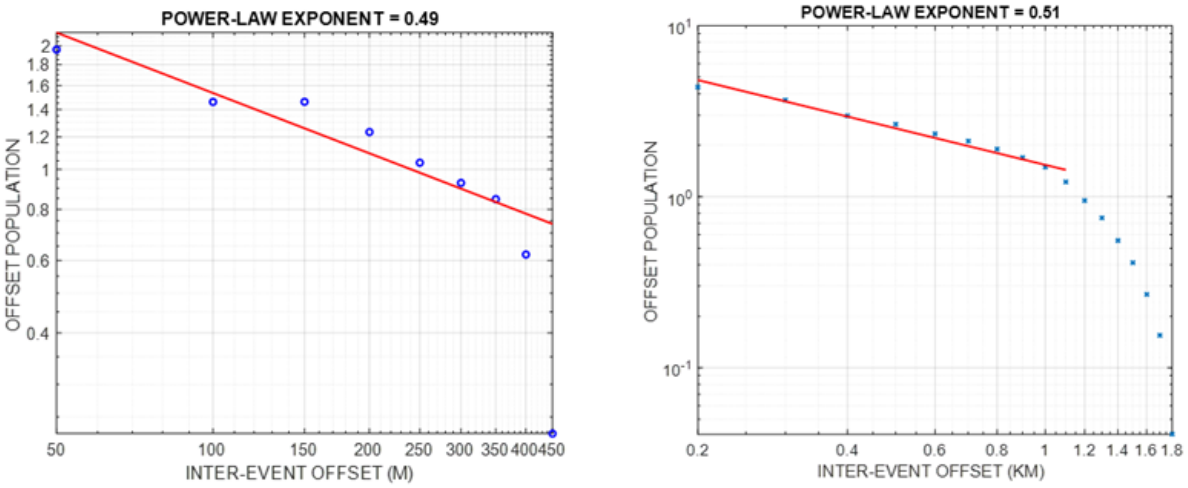


**Figure 5: Power-law spatial correlation functions for distributions of induced seismic in Finnish basement (left, [15]) and ambient seismicity in a convective geothermal field in Indonesia (right, [17]).**

## 4. DERIVING SPATIAL CORRELATION FUNCTION $\Gamma(R) \sim 1/R^{1/2}$ FROM SPECTRAL POWER-LAW SCALING EMPIRIC $S_\Phi(K) \sim 1/K$

Figs 6-8 summarise the numerical exercise in which 2D permeability distributions $\kappa(x,y)$ derived from a range of porosity spatial correlations given by generalizing the crustal fluid flow empiric (I), $S_\varphi(k) \sim 1/k^m$, $0 < m < 2$, are processed by the two-point correlation function to determine the associated value of the power-law scaling exponent $n$, $\Gamma_\kappa(r) \sim 1/r^n$, controlled by porosity spatial correlation parameter $m$.

Fig 6 gives four samples of spatial distributions of permeability highs $\kappa(x,y)$ generated by the sequence of porosity spatial correlation exponent $m$ = [0.25 0.8 1.1 1.7]. Each distribution is a slice from a 3D permeability $\kappa(x,y,z)$ distribution associated with spatially correlated 3D random porosity field $\varphi(x,y,z)$ through crustal empirics (II)-(III), $\kappa \sim \exp(\alpha\varphi)$. Fig 7 shows representative porosity-field well-log spectral scaling in x-, y-, and z-directions.

Fig 8 displays the $n$-$m$ exponent parameter trend established by the sequence parameter values illustrated by Figs 6-7. Error bars indicate the range of statistical fluctuations for exponent $n$ across the range of planar sections through the 3D permeability field for each value of exponent $m$. The red circle indicates that the observed spectral-scaling spatial correlation exponent $m \sim 1$ characteristic of crustal empiric (I) corresponds to the two-point spatial correlation exponent $n \sim 1/2$ characteristic of induced seismicity at 6km depth in Finland [15] shown in Fig 5 (left) and the sample of Indonesia geothermal field ambient seismicity shown in Fig 5 (right).

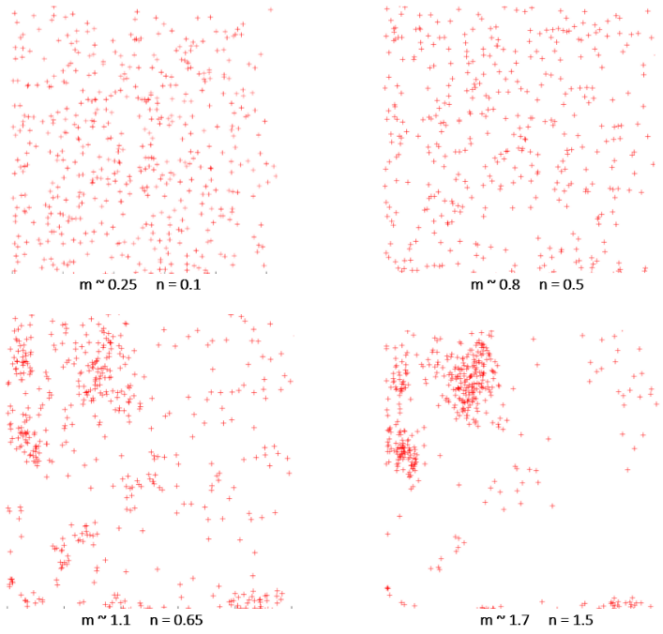


**Figure 6: Spatial distribution of permeability highs for four degrees of porosity spatial correlation governed by spectral power-law scaping exponent m, $P_\varphi(k) \sim 1/k^m$. From upper left to lower right, exponents are m ~ 0.2, 0.8, 1.1, 1.7. The corresponding two-point spatial correlation function power-law scaling exponents, $\Gamma_\kappa(r) \sim 1/r^n$, are n ~ 0.1, 0.5, 0.65, 1.5. The power-law scaling exponent pairs observed in ambient and induced seismicity are 0.47 < n < 0.65 corresponding to porosity-controlled permeability distributions generated by observed porosity power-law scaling exponent m ~ 1.1 ± 0.1**

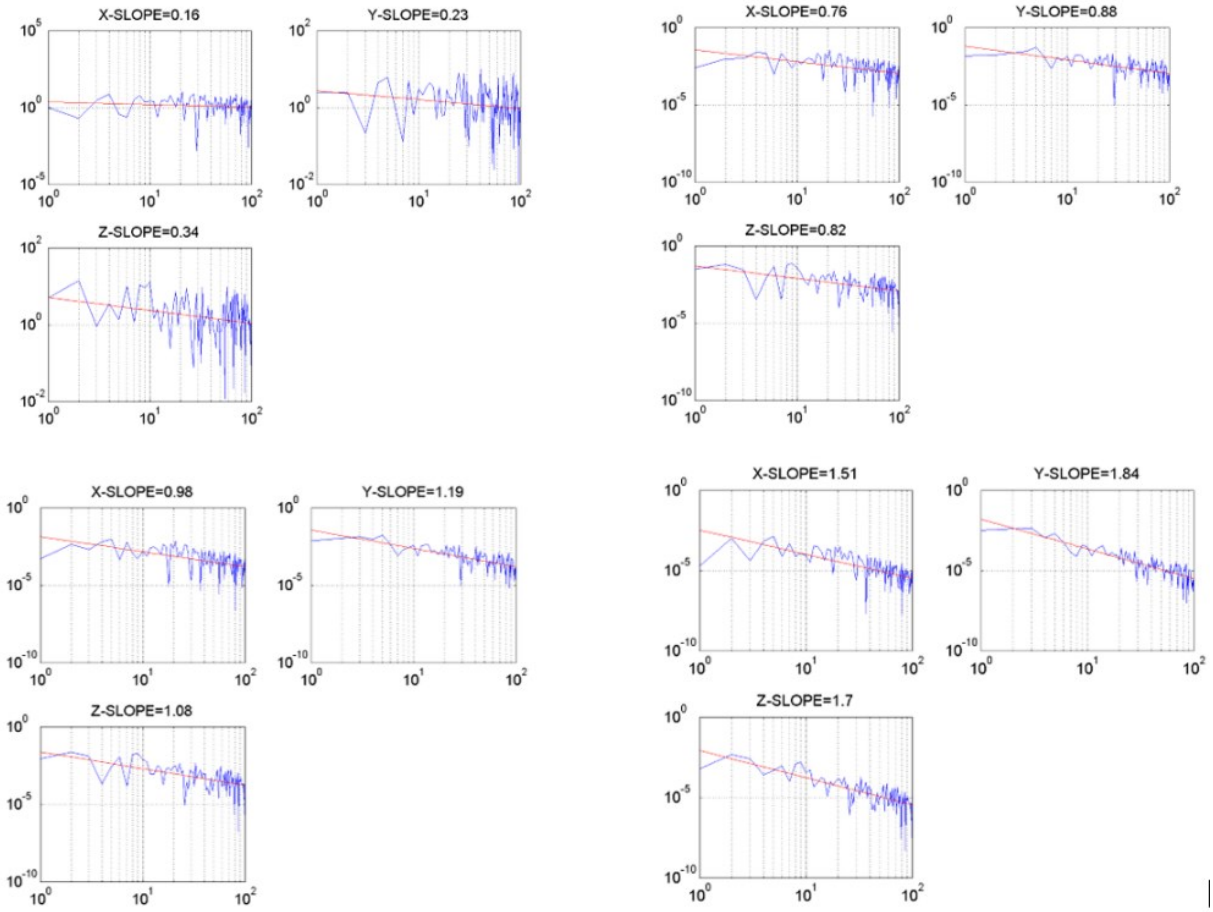


**Figure 7: Loglog plots of power-law scaling spectra for 3D porosity distributions φ(x,y,z) used to create Fig 6 sample 2D crustal permeability section distributions κ(x,y). Permeability is given by empirical relation κ ~ exp(αφ), with empirical parameter α fixed by condition $\alpha\underline{\varphi} \sim 3$ for mean porosity $\underline{\varphi}$. Power-law spectral scaling exponents for well-log traces along x, y, and z axes are given above each spectral loglog plot.**

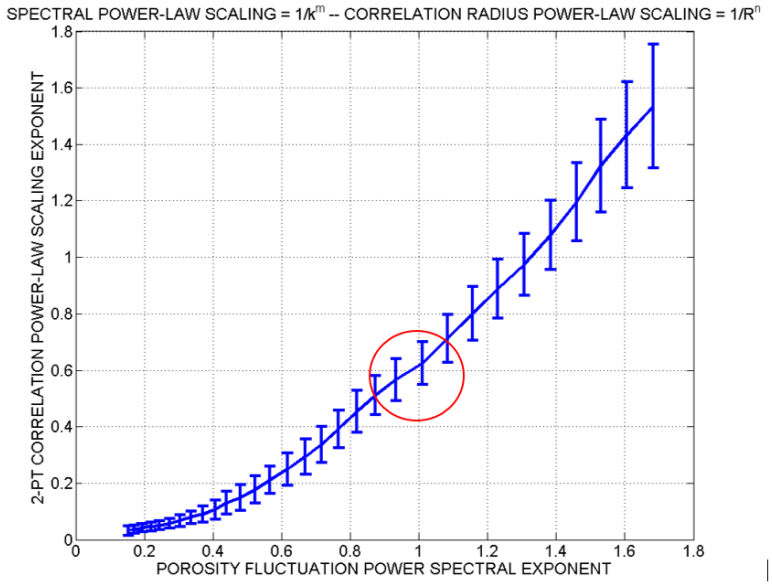


**Figure 8: Plot of dependency of two-point spatial correlation function power-law scaling exponent n, $\Gamma_\kappa(r) \sim 1/r^n$, on degree of porosity spatial correlated governed by spectral power-law scaling exponent m $S_\varphi(k) \sim 1/k^m$. The greater the degree of porosity spatial correlation, the greater the degree of permeability clustering, and by quantitative extension, the greater the degree of microseismicity clustering. Observed ambient and induced seismicity clustering corresponds to the observed degree of porosity spatial correlation.**

## 5. DISCUSSION

Fig 8 summarises a numerical exercise in which a permeability two-point spatial correlation function $\Gamma_\kappa(r) \sim 1/r^n$, parameterised by exponent $n$, is controlled by a porosity spectral spatial correlation condition $S_\varphi(k) \sim 1/k^m$, parameterised by exponent $m$. The red circle of Fig 8 establishes the clear statistical result that the empirical porosity power-law scaling spectral correlation exponent $m \sim 1$ induces an observed two-point power-law spatial correlation in permeability exponent $n \sim ½$. We now consider physical aspects of crustal seismic processes to apply the Fig 8 statistical result to observations of induced microseismicity in Finnish basement [15] and ambient microseismicity in an Indonesian geothermal field [17].

To this end, we note that, in comparison with crustal seismicity at large, the observed Finnish basement induced seismicity has an unusually large number of smaller magnitude events relative to the number of large magnitude events. The observations pictured in Fig 9 give the 60-day temporal progress of the empirical Gutenberg-Richter scaling law exponent $b$ that parameterises the ratio $N(m_1)/N(m_2) = 10^{-b(m1-m2)}$ of the number of magnitude $m_1$ seismic events to the number of magnitude $m_2$ seismic events. The larger the value of $b$, the greater the number of smaller magnitude events relative to the number of larger magnitude events [15].

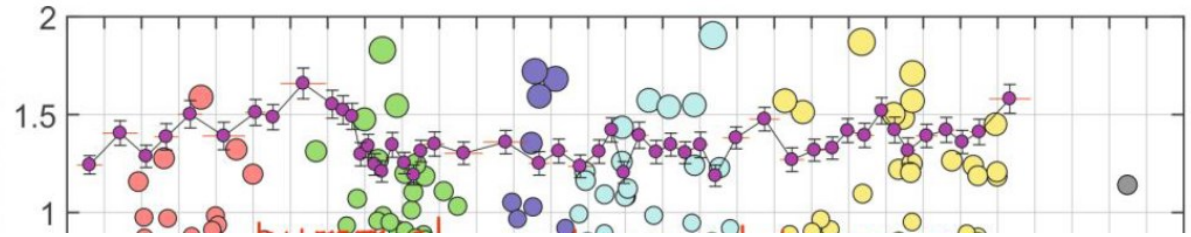


**Figure 9: Time plot of seismic event b-values (magenta filled circles with error bars) derived from Finnish basement rock stimulation seismicity recorded between 04 June and 03 August 2018. Remaining filled circles mark the occurrence of stimulation seismic events of magnitude range ~1 < m < 2 in five stimulation phases followed by two weeks of quiescence [15].**

Recognising the Gutenberg-Richter scaling exponent $b$ as a form of fractal dimension $D$, we adopt the simplest geometric interpretation of seismic events as slip on planar surface of characteristic dimension $L$ [31-35]. For a seismic event of slip $\Delta L$ on a plane of area $A = L^2$ with strain relief $\varepsilon \equiv \Delta L/L$ in a crustal volume of shear modulus G, the seismic moment is $M \equiv \Delta L \cdot A \cdot G$. Seismic moment is in turn related to seismic magnitude by $M(m) \propto 10^{cm}$, $c = 3/2$, and event frequency by $N(m) \propto 10^{-bm}$. If the observed seismicity occurs in a crustal volume subject to elastic stress σ, the elastic energy $E(m)$ associated magnitude $m$ events is $E(m) = \sigma/G$ $M(m) = \sigma \Delta L \cdot L^2 = \sigma\varepsilon L^3$. If the stimulated crustal volume is characterized by a constant confining stress σ and constant strain release ε, then the slip event energy is fixed by the characteristic slip dimension $L$.

Assuming for simplicity that the seismic events in our crustal volume have constant characteristic strain relief ε, event energies are related via their dimension $L$ to event magnitude $m$ as $E(m) \propto 10^{cm}$. It follows that within the crustal volume the overall seismic energy release for events of dimension $L$ and magnitude $m$ is given by $E(m)N(m) \propto 10^{(c-b)m}$. If event size exponential coefficient $c$ is of the same order as the event number exponential coefficient $b$, i.e., $c \sim b$, then the energy partition across the range of seismic dimensions and magnitudes $E(m)N(m)$ is independent of event size $L$ and magnitude $m$. That is, the smaller event energies are balanced by the greater number of small events. As seen ni Fig 9, the $c \sim b$ condition appears to be approximately observed at the

Finnish basement induced seismicity crustal volume [15]. A similar condition appears to apply to the 2006 Basel induced seismicity crustal volume [35].

In view of Fig 9, we suggest that careful, steady, sustained fluid injection stimulation of crustal basement volumes is controlled to a considerable degree by either/both existing and/or pre-existing but now fossilized crustal permeability structures described by crustal fluid flow empirics (I)-(III). As such, careful, steady fluid injection stimulation may be seen as a quasi-equilibrium process which activates or reactivates flow structures generated by long-term crustal fluid-rock interactions [2-9]. As these long-term rock-fluid interactions partition crustal deformation damage and its associated permeability pathways over a large range of scale lengths, so present-day controlled stimulation fluid injection triggers equipartitioned seismic energy release across the entire range of scale lengths.

Given the evidence of seismic event scaling to magnitude values of order $m \sim -2$ and smaller, it is plausible that fluid-flow-activated seismic events are ever-present in time and space so that multi-channel seismic sensor arrays recording over sufficiently long periods of time can detect and map the associated flow structures [10-14]. It is interesting to note that multi-channel seismic arrays document in time and space the effects of solid-earth-tide strain deformation of order $10^{-8}$ in volcanic terrains at depths to 2km [36]. Such crustal strains exerted on crustal volumes of order $1m^3$ involve crustal deformation energy of order $E \sim \sigma\varepsilon L^3 \sim 100MPa \times 10^{-8} \times 1m^3 \sim 1J$, equivalent in energy to $m \sim -3$ ''nano-to-pico-seismic'' slip events.

From the collective seismic sensor data given by [10-14, 15, 17, 35-36] placed in the context of crustal empirics (I)-(III), spatial correlation statistics result Fig 8, and general seismic scaling over orders of seismic event magnitude, it is observationally almost certain that fluid-mediated interactions in km-depth crustal volumes generate low-level fluid-flow-specific seismic signals that can be detected and processed by surface sensor arrays. Application of such flow-structure imaging stands to greatly benefit the production of electrical power from convective geothermal systems.

**REFERENCES**


[1] Malin P, Leary P, Shalev E, Rugis J, Valles B, Boese C, Andrews J & Geiser P (2015) Flow Lognormality and Spatial Correlation in Crustal Reservoirs: II – Where-to-Drill Guidance via Acoustic/Seismic Imaging, WGC2015, 19-24 April, Melbourne AU.

[2] Leary PC (1997) Rock as a critical-point system and the inherent implausibility of reliable earthquake prediction, *Geophysical Journal International,*131, 451-466.

[3] Leary PC (2002) Fractures and physical heterogeneity in crustal rock, in *Heterogeneity of the Crust and Upper Mantle – Nature, Scaling and Seismic Properties*, JA Goff & K Holliger eds., Kluwer Academic/Plenum Publishers, New York, 155-186.

[4] Leary PC & Al-Kindy F (2002) Power-law scaling of spatially correlated porosity and log(permeability) sequences from northcentral North Sea Brae oilfield well core, *Geophysical Journal International 148*, 426-442.

[5] Leary P, Malin P & Niemi R (2017) Finite-Element Modelling of Wellbore-Observed Fracture-Borne Heat Advection – Application to EGS Stimulation in Basement Rock, *41st Workshop Geothermal Reservoir Engineering*, Stanford University, February 13-15, SGP-TR-212.

[6] Leary P, Malin P & Niemi R (2017) Fluid flow & heat transport computation for power-law scaling poroperm media, *Geofluids*, Volume 2017, https://doi.org/10.1155/2017/9687325

[7] Leary P, Malin P, Saarno T & Kukkonen I (2017) Prospects for Assessing Enhanced Geothermal System (EGS) Basement Rock Flow Stimulation by Wellbore Temperature Data, *Energies*, 10, 1979; doi:10.3390/en10121979

[8] Leary P, Malin P, Saarno T & Kukkonen I (2018) $\alpha\varphi \sim \alpha\varphi$ crit – Basement Rock EGS as Extension of Reservoir Rock Flow Processes, *43rd Workshop on Geothermal Reservoir Engineering,* Stanford University, February 12-14, 2018 SGP-TR-213.

[9] Leary P, Malin P, Saarno T, Heikkinen P & Diningrat W (2019) Coupling Crustal Seismicity to Crustal Permeability – Power-Law Spatial Correlation for EGS-Induced and Hydrothermal Seismicity, *44th Workshop on Geothermal Reservoir Engineering,* Stanford University, February 11-13, 2019 SGP-TR-2141.

[10] Geiser P, Vermilye J, Scammell R & Roecker S (2006) Seismic used to directly map reservoir permeability fields. *Oil & Gas Journal*.

[11] Geiser P, Lacazette A & Vermilye J (2012) Beyond "dots in a box", First Break, 30, 63 – 69.

[12] Geiser P & Leary P (2014) Tomographic Fracture Imaging (TFI): Direct 5D Mapping of Transmissive Fracture/fault Zones Using Seismic Emission Tomography (SET), *39th Workshop on Geothermal Reservoir Engineering*, Stanford University, February 24-26, 2014 SGP-TR-2021

[13] Ross J, Parrott K, Vermilye J & Klaus A (2017) Tomographic fracture imaging: Examples of induced fracture and reservoir-scale observations during wellbore stimulations, Niobrara and Bakken plays, USA, *The Leading Edge*, http://dx.doi.org/10.1190/tle36050437.1.

[14] Sicking C, Vermilye J & Yaner A (2017) Forecasting reservoir performance by mapping seismic emissions, *Interpretation*, Vol. 5, No. 4; http://dx.doi.org/10.1190/INT-2015-0198.1.

[15] Kwiatek G, Saarno T, Ader T, Bluemle F, Bohnhoff M, Chendorain M, Dresen G, Heikkinen P, Kukkonen I, Leary P, Leonhardt M, Malin P, Martínez-Garzón P, Passmore K, Passmore P, Valenzuela S & Wollin C (2019) Controlling fluid-induced seismicity during a 6.1-km-deep geothermal stimulation in Finland, *Science Advances* 01 May 2019: Vol. 5, no. 5, eaav7224 DOI: 10.1126/sciadv.aav7224.

[16] Yaglom AM (1962) *An Introduction to the Theory of Stationary Random Functions*, Englewood Cliffs, New Jersey: Prentice–Hall; §§8-10; eqs (2.66)-(2.69).

[17] Muchlis VA, Sule R, Nugraha AD & Kusnadi Y (2015) Reservoir Characterization Based on Hypocenter Location Analysis and 3-D Seismic Velocities, Proceedings World Geothermal Congress 2015 Melbourne, Australia, 19-25 April 2015.

[18] Muskat M & Botset HG (1931) Flow of gas through porous materials, *Journal of Applied Physics* 1, 27 (1931); doi: 10.1063/1.1744983.

[19] Wyckoff RD, Botset HG, Muskat M & Reed DW (1933) The Measurement of the Permeability of Porous Media for Homogeneous Fluids, *Review of Scientific Instruments* 4, 394; doi: 10.1063/1.1749155.

[20] Muskat M (1937) *The Flow of Homogeneous Fluids through Porous Media*; McGraw-Hill: New York, NY, USA, p. 763.

[21] Hubbert MK (1941) Motion of ground water, *Transactions of New York Academy of Science*, 3, 39–55.

[22] Hubbert MK (1957) Darcy's law and the field equations of the flow of underground fluids, *International Association of Scientific Hydrology, Bulletin*, *2:1*, 23-59; doi: 10.1080/02626665709493062.
[23] Bear J (1972) Dynamics of Fluids in Porous Media, American Elsevier: New York, NY, USA.

[24] Jensen JL, Lake LW, Corbett PWM & Goggin DJ (1997) *Statistics for Petroleum Engineers and Geoscientists*, Prentice-Hall, New Jersey, pp390.
[25] Theis CV (1935) The relation between the lowering of the piezometric surface and the rate and duration of discharge of a well using ground-water storage, *Transactions American Geophysical Union*.
[26] Warren JE & Root PJ (1963) The behavior of naturally fractured reservoirs, *Society of Petroleum Engineers Journal*, pp. 245–255.
[27] Pruess K, Oldenburg C & Moridis GJ (2012) TOUGH2 User's Guide, Version 2.1, Tech. Rep. LBNL-43134, Lawrence Berkeley National Laboratory.
[28] Kagan YY & Knopoff L (1980) Spatial distribution of earthquakes: the two-point correlation function, *Geophysical Journal Royal Astronomical Society* 62, 303-320.
[29] *Totsuji H & Kihara T* (1969) The correlation function for the distribution of galaxies, *Publications of the Astronomical Society* of *Japan*, vol. *21*, p.*221*.
[30] Landau LD & Lifshitz EM (1980) *Statistical Physics*, Pergamon Press, Oxford.
[31] Aki, K., 1981. A probabilistic synthesis of precursory phenomena, in *Earthquake Prediction: An International Review,* Maurice Ewing Ser., vol. 4, pp. 566-574, eds Simpson, D. W. & Richards, P. G., AGU, Washington, DC.
[32] King G (1983) The accommodation of large strains in the upper lithosphere *of* the earth and other solids by self-similar fault systems: The geometrical origin of b-value, *Pure and Applied Geophysics* 121(5):761-815; DOI: 10.1007/BF02590182.
[33] Hirata T, Satoh T & Ito K (1987) Fractal structure of spatial distribution of microfracturing in rock, *Geophys. J. R. astr.*
[34] Hirata T & Imoto M (1991) Multifractal analysis of spatial distribution of microearthquakes in the Kanto region, *Geophys. J. int.* (1991) 107, 155-162.
[35] Bachmann CE, Wiemer S, Goertz-Allmann BP & Woessner J (2012) Influence of pore-pressure on the event-size distribution of induced earthquakes. *Geophys. Res. Lett.* **39**; doi:10.1029/2012GL051480.
[36] Mao S, Campillo M, van der Hilst R D, Brenguier F, Stehly L & Hillers G (2019). High temporal resolution monitoring of small variations in crustal strain by dense seismic arrays, *Geophysical Research Letters* 46,128–137; https://doi.org/10.1029/2018GL079944.

**Appendix – Matlab two-point correlation function**

```
% [ corrfun r rw] = twopointcorr( x,y,dr)   Developed by Ilya Valmianski   email: ivalmian@ucsd.edu
% Computes the two-point correlation function over a 2D lattice of a fixed width and height
% x - list of x coordinates of points   y - list of y coordinates of points   dr - binning distance for successive circles
% corrfun – two-point correlation function   r – radial values for coordfun   rw - number of particles for particular r value
% Low rw means corrfun is unreliable at that r.
%
function [corrfun r rw] = twopointcorr( x,y,dr)
   x = reshape(squeeze(x),[length(x) 1]); y = reshape(squeeze(y),[length(y) 1]);
   % real height/width; number particles; largest radius
   width = max(x)-min(x); height = max(y)-min(y); totalPart = length(x); maxR = sqrt((width/2)^2 + (height/2)^2);
   %r bins, area bins   default blksize = 1000
   r = dr:dr:maxR; av_dens = totalPart/width/height; rareas = ((2*pi*r* dr)*av_dens); blksize = 1000;
   corrfun = r*0; rw = r*0;  % allocate space for corrfun/rw
   numsteps = ceil(totalPart / blksize);  % number of steps to be considered
   for j = 1:numsteps         % loop through all particles, compute correlation function
      indi = (j-1)*blksize+1; indf = min(totalPart,j*blksize);
      [corrfunArr rwArr] = arrayfun(@ (xj,yj) onePartCorr(xj,yj,x,y,r,rareas),x(indi:indf),y(indi:indf),'UniformOutput',false);
      rw = rw + sum(cell2mat(rwArr),1); corrfun =  corrfun + sum(cell2mat(corrfunArr),1);
   end
   corrfun = corrfun ./rw;corrfun = corrfun(rw~=0); r = r(rw~=0);rw = rw(rw~=0);   % truncate values with no contributions
end
%
function [corrfun rw] = onePartCorr(xj,yj,x,y,r,rareas)  % compute radii in (xj,yj)-centered coordinates
   rho=hypot(x-xj,y-yj);rho=rho(logical(rho))';
   maxRho = min([max(x)-xj,xj-min(x),max(y)-yj,yj-min(y)]);  % compute maximum unbiased rho
   rho=rho(rho<maxRho);   % truncate to highest unbiased rho
   rw=r*0; rw(r<maxRho)=1; % indicate for which r-values correlation function is computed
   count=histc( rho,[-inf r]'); count=count(2:end);  % compute count with correct binning
   corrfun = count./rareas;  % normalize density
end
```